Coherent Rabi response of a charge-phase qubit under microwave irradiation

V. I. Shnyrkov,[1,*] D. Born,[2,†] A. A. Soroka,[3] and W. Krech[2]

[1]*B. Verkin Institute for Low Temperature Physics and Engineering, National Academy of Sciences of Ukraine, Avenue Lenina 47, Kharkov 61103, Ukraine*

[2]*Institute of Solid State Physics, Friedrich Schiller University, Helmholtzweg 5, D-07743 Jena, Germany*

[3]*National Science Center, Kharkov Institute of Physics and Technology, Akhiezer Institute for Theoretical Physics, Street Akademicheskaya 1, 61108 Kharkov, Ukraine*

(Received 17 October 2008; revised manuscript received 11 March 2009; published 22 May 2009)

We report on radio-frequency (rf) measurements of the charge-phase qubit being under continuous microwave irradiation in the state of weak coupling to a radio-frequency tank circuit. We studied the rf impedance dependence on the two important parameters such as the power of microwave irradiation, whose frequency is close to the gap between the two lowest qubit energy levels, and the temperature of the internal heat bath. We have found that backaction effects of the qubit on the rf tank and vice versa, tank on the qubit, lead to a negative as well as a positive real part of the qubit impedance Re $Z(\omega)$ seen by the tank. We have implemented noise spectroscopy measurements for direct impedance readout at the extreme points corresponding to maximum voltage response and obtained absolute values of about 0.017 Ω for the negative and positive Re $Z(\omega)$. Our results demonstrate the existence and persistence of the coherent single- and multiphoton Rabi dynamics of the qubit with both negative and positive dynamic resistances inserted into the tank in the temperature range of 10–200 mK.

DOI: 10.1103/PhysRevB.79.184522 PACS number(s): 74.25.Nf, 42.50.Dv, 85.25.Am

I. INTRODUCTION

Nowadays, the problem of building a new class of information signal detectors based on solid-state Josephson qubits, in which coherent phenomena such as single- and multiphoton Rabi oscillations occur, is under intensive discussion.[1–7] The behavior of these detectors would essentially differ from that of quantum devices utilizing nonlinear effects of macroscopic quantum tunneling, macroscopic resonant tunneling, and superposition of macroscopic states[8–13] by the presence of intrinsic generation in the qubit at the Rabi frequency. The variation in ground and excited levels population of the qubit with the Rabi frequency results in a periodic alteration of the magnitude and sign of the qubit reactive parameter. Similar to the known classical electrodynamics of Josephson junction in a resonator giving rise to the effects of parametric amplification,[14–16] the interaction of a weak signal from the tank circuit with Rabi oscillations in the qubit may lead to parametric amplification (attenuation) effects, i.e., negative (positive) resistance being inserted from the qubit into the tank circuit.[17–19] The amplitude of these effects will depend on the qubit decoherence time τ_φ (Rabi oscillations frequency band); the latter must exceed the period of oscillations in the tank circuit coupled with the qubit, $\tau_\varphi > T = 2\pi/\omega_T$, where ω_T is the tank circuit resonant frequency.

It was shown[20,21] that a qubit placed in microwave (MW) field might show Sisyphus cooling effects[21–23] in the opposite limit $\tau_\varphi < T \approx \tau_R$, i.e., when the qubit decoherence time was less than the LC tank circuit oscillation period which was about the relaxation time τ_R. The observation of the negative resistance inserted by the qubit into the tank circuit is possible in both cases. However, the resistance value and its dependence on temperature, frequency, and microwave power will substantially differ. In both cases, the characteristics of the qubit-detector system will depend on the qubit's effective temperature T_{eff}, which is contributed by the measurement process itself, the physical temperature of the bath T_{bath}, the quality of thermalization[24] of the qubit input circuit (gates), etc. Note that in a region of large T_{eff} values, the observation of complicated classical electrodynamics associated with so-called pseudo-Rabi oscillations is possible.[25]

The aim of this work is to analyze experimentally coherent processes in a charge-phase qubit[26,27] being under continuous microwave irradiation in the state of weak coupling to a radio-frequency tank circuit. It is important to note here that our experiment is similar but not identical to that of Ref. 21. In this paper, we address the problem of coherent single- and multiphoton Rabi dynamics of the charge-phase qubit with $\tau_\varphi > T$ in a wide temperature range. The direct observation of absorption and irradiation properties of a strongly driven qubit coupled to a rf tank circuit, being of fundamental interest, also has potential applications to quantum detectors based on charge-flux qubits with self-Rabi frequency pumping.

The paper is organized as follows. In Sec. II, the theoretical description of a strongly driven charge-phase qubit coupled to an rf tank detector and the analysis of measured output functions are given. The main Sec. III is devoted to the detailed experimental investigation of coherent single- and multiphoton Rabi dynamics of the strongly driven charge-phase qubit probed by an rf tank detector.

II. SYSTEM OF CHARGE-PHASE QUBIT AND TANK CIRCUIT

The charge-phase qubit (Fig. 1) is topologically a single-junction rf superconducting quantum interference device (SQUID) whose Josephson junction is replaced by a single-Cooper-pair transistor.[26–29] The latter consists of two mesos-

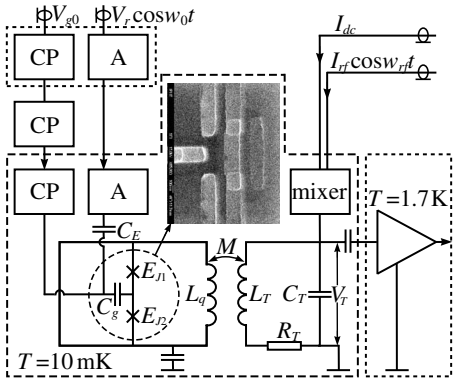

FIG. 1. Circuit diagram of the charge-phase measurement system. The components situated at the lowest temperature are shown in the dashed box. The qubit and *LC* tank circuit parameters are $L_q=(0.9\pm0.045)$ nH, $I_{c1,2}\approx 100$ nA, $C_{J1,2}\approx 2.0$ fF, $C_g=(0.18\pm0.02)$ fF, $C_T=(165\pm5)$ pF, $L_T=(0.173\pm0.003)$ μH, $\omega_T/2\pi=(29.8\pm0.05)$ MHz, $R_T=(0.092\pm0.002)$ Ω, and $Q_0=350\pm2$; $M=(0.365\pm0.005)$ nH and the parameter $k^2Q_0=0.3\pm0.03$. The preamplifier and the part of the tank circuit placed on 1 K pot are shown in the dotted boxes. All the electric lines are equipped with copper powder (CP) filters and attenuators (A).

copic junctions with Josephson energies E_{J1}, E_{J2} and capacitances C_1, C_2 coupled by a small island. The Hamiltonian of the charge-phase qubit in the eigenstate basis within the two-level approximation $[E_{\rm CP}\gg\varepsilon_J(\delta)]$ and the small-inductance limit reads as[27,30–32]

$$\hat{H}_q=\frac{1}{2}\Delta E\hat{\sigma}_z=\frac{1}{2}[\varepsilon_J^2(\delta)+D^2(n_g)]^{1/2}\hat{\sigma}_z, \tag{1}$$

where the effective Josephson energy $\varepsilon_J(\delta)=(E_{J1}^2+E_{J2}^2+2E_{J1}E_{J2}\cos\delta)^{1/2}$ is a function of the total phase bias across both junctions $\delta=\varphi_1+\varphi_2$ (φ_1 and φ_2 are phase differences at the individual junctions); $D\equiv E_{\rm CP}(1-n_g)$, parameter $n_g=C_gV_g/e$ characterizes the polarization charge en_g in the island controlled by the gate voltage V_g via the charge-gate capacitance C_g, and $E_{\rm CP}=(2e)^2/2C_\Sigma$ is the two-electron Coulomb energy of the island expressed through its total capacitance $C_\Sigma=C_1+C_2+C_g$ regarding the rest of the system. The inductance L_q of the qubit loop is assumed to conform to the small-inductance limit (typically $L_qI_c/\Phi_0\sim10^{-2}$, $\Phi_0=h/2e$ is the flux quantum), so that the total flux through the qubit loop $\Phi\approx\Phi_e$, $\delta\approx2\pi\Phi_e/\Phi_0$, and the potential (Josephson) energy of the qubit is periodic on Φ. Thus, the charge-phase qubit design permits the implementation of an *in situ* control of Josephson coupling energy $\varepsilon_J(\delta)$ by means of external magnetic flux Φ_e and the effective charging energy $D(n_g)$ by gate voltage V_g. The current operator of an isolated qubit corresponding to the Hamiltonian (1) is given by[27,30–32]

$$\hat{I}=\frac{2e}{\hbar}\frac{\partial\hat{H}_q}{\partial\delta}=I_q\hat{\sigma}_z,\quad I_q(n_g,\delta)=\frac{e}{\hbar}\frac{E_{J1}E_{J2}\sin\delta}{\Delta E(n_g,\delta)}, \tag{2}$$

so that its basis states are discriminated by the two oppositely circulating in the qubit loop supercurrents I_q that correspond to the ground and the excited qubit energy levels.

In the general case, at arbitrary ratio of the Josephson and charging energies $\varepsilon_J(\delta)/E_{\rm CP}$ [while the two-level approximation (1) is determined by $\varepsilon_J(\delta)/E_{\rm CP}\ll1$], the energy spectrum and eigenfunctions of the charge-phase qubit are given, respectively, by the Bloch bands $E_n(q,\delta)$ and the Bloch wave functions $|q,\delta;n\rangle$ ($n=0,1,2\ldots$ is the band index and $q=en_g$ is the quasicharge) that are numerical solutions of Schrödinger equation with Hamiltonian containing all the charge states and a periodic Josephson potential.[26,29] Then the lowest two energy levels $n=0,1$ form the basis of the charge-phase qubit, so that $\hat{H}_q=(1/2)\Delta E\hat{\sigma}_z$, where $\Delta E=E_1(n_g,\delta)-E_0(n_g,\delta)$ is the energy gap between the two lowest qubit levels.

In our experiments, the qubit is driven by coupling the microwave field of frequency ω_0 and amplitude V_r to a voltage gate with constant voltage component V_{g0}, $V_g=V_{g0}+V_r\cos\omega_0t$, and its dynamical properties are probed by the well-known rf SQUID impedance measuring technique[33,34] (IMT) following the conception of weak continuous quantum measurements.[17,35–38] In the IMT, the qubit is inductively coupled to a high-quality tank circuit serving as a linear detector. For the tank circuit driven by a small-amplitude external rf-bias current $I_{\rm rf}\cos\omega_{\rm rf}t$, the measured output functions are the amplitude of the voltage oscillations V_T and the voltage-current phase shift α_T. Also, the spectrum of voltage fluctuations $S_V(\omega)$ in the undriven tank can be sensitive to qubit dynamics (the noise spectroscopy method).

The IMT weak continuous measurements were effectively used for microwave spectroscopy and characterization of charge-phase qubits.[31,32] There, the resonant response of the qubit to microwave irradiation was observed through a change in the average qubit Josephson inductance making contribution to the reactive part of the tank impedance. Essentially, different effects were predicted in Ref. 17, when at resonant microwave irradiation there exist coherent low-frequency (Rabi-type) oscillations in a qubit with frequency nearby the tank resonant frequency. Then damping and amplification of the voltage signal V_T, with respective modification of the spectrum of voltage fluctuations $S_V(\omega)$ in the undriven tank and its quality factor, should be observed owing to the insertion of positive or negative dynamic active impedance (resistance) into the tank circuit from a qubit. These phenomena enable probing the coherent properties of qubits necessary for quantum manipulations.

In the presence of the qubit, at the resonant condition $\omega_{\rm rf}=\omega_T$ of driving the tank, the expressions for its effective damping rate $\bar{\gamma}_T$, the resonant frequency $\bar{\omega}_T$, the amplitude of the voltage oscillations V_T, and the voltage-current phase shift α_T have the form[17,18]

$$\bar{\gamma}_T=\gamma_T+k^2L_qI_q^2\omega_T\chi_{zz}''(\omega_T), \tag{3a}$$

$$\bar{\omega}_T=\omega_T\sqrt{1-k^2L_qI_q^2\chi_{zz}'(\omega_T)}, \tag{3b}$$

$$V_T=\frac{I_{\rm rf}}{C_T}\frac{1}{\sqrt{[k^2L_qI_q^2\omega_T\chi_{zz}'(\omega_T)]^2+\bar{\gamma}_T^2}}, \tag{3c}$$

$$\tan \alpha_T = -k^2 L_q I_q^2 \frac{\omega_T}{\bar{\gamma}_T} \chi'_{zz}(\omega_T), \tag{3d}$$

where γ_T is the own damping rate of the tank, $k=M/\sqrt{L_T L_q} \ll 1$ is the coupling coefficient, M is the mutual qubit-tank inductance, L_T and C_T are the inductance and capacitance of the tank, respectively, and $\chi'_{zz}(\omega), \chi''_{zz}(\omega)$ are the real and imaginary parts of the qubit magnetic susceptibility $\chi_{zz}(\omega)$. The latter is defined by the relation $(d\langle \hat{I} \rangle / dt)_\omega = \chi_{zz}(\omega) M I_q^2 (dI_T/dt)_\omega$ and describes a low-frequency response of the qubit to a tank probing signal. The rate of absorbtion of weak signal energy by a qubit from a tank $U(\omega)=(1/2)\omega\chi''_{zz}(\omega)(MI_qI_T)^2$ ($I_T=V_T/\omega L_T$ is the current in the tank), according to properties of generalized susceptibility.[39] Thus, the function $\chi''_{zz}(\omega)$ defines the absorption $[\chi''_{zz}(\omega)>0]$ and irradiation $[\chi''_{zz}(\omega)<0]$ properties of a driven qubit coupled to rf tank detector.

Renormalizations (3a) and (3b) of the tank parameters $\bar{\gamma}_T, \bar{\omega}_T$ at resonance ($\omega=\omega_T$) involves the renormalization of the tank quality factor

$$Q = \frac{\bar{\omega}_T}{\bar{\gamma}_T} = \frac{\bar{\omega}_T \bar{L}_T}{\bar{R}_T} = \frac{\bar{\omega}_T (L_T + L_q)}{R_T + R_q}, \quad \bar{\omega}_T = (\bar{L}_T C_T)^{-1/2},$$

$$L_q \approx L_T k^2 L_q I_q^2 \chi'_{zz}(\omega_T), \quad R_q \approx \omega_T L_T k^2 L_q I_q^2 \chi''_{zz}(\omega_T), \tag{4}$$

where $\bar{L}_T=L_T+L_q$ is the effective inductance of the tank including inserted from the qubit inductance L_q, and $\bar{R}_T=R_T+R_q$ is the effective resistance of the tank including inserted from the qubit resistance R_q [$R_q(\omega)=\mathrm{Re}\, Z(\omega)$, where $Z(\omega)$ is the qubit impedance seen by the tank]. The characteristic impedance of the tank at resonance is

$$R_c = \frac{V_T}{I_{\mathrm{rf}}} = \frac{Q}{\bar{\omega}_T C_T} = Q^2 \bar{R}_T = \frac{\bar{L}_T}{\bar{R}_T C_T},$$

so that the tank voltage V_T is inversely proportional to the effective tank resistance $\bar{R}_T$. The Lorentzian-shaped voltage fluctuations spectrum $S_V(\omega)$ in the tank is characterized by the renormalized quality factor (4).

For the special case of charge-phase qubits, the theory of Rabi oscillations and low-frequency qubit response have been investigated in Ref. 18. The Rabi frequency Ω_R of coherent low-frequency oscillations generated at near-resonant driving of the charge-phase qubit by microwave field reads as[18]

$$\Omega_R = \sqrt{\Omega_0^2 + \varepsilon^2}, \quad \varepsilon = \omega_g - n\omega_0, \quad \omega_g = \Delta E/\hbar, \quad |\varepsilon| \ll \omega_0,$$

$$\Omega_0 = n\omega_0 \tan \eta J_n(\alpha), \quad \alpha = \frac{2eV_r}{\hbar\omega_0}\frac{C_g}{C_\Sigma}\cos \eta, \tag{5}$$

where Ω_0 is the core n-photon Rabi frequency, $\tan \eta = \varepsilon_J(\delta)/D(n_g) \lesssim 1$. The most essential in our context low-frequency parts of the functions $\chi'_{zz}(\omega), \chi''_{zz}(\omega)$ in the presence of Rabi oscillations have the form[18]

$$\chi'_{zz}(\omega) = \frac{P_0}{\hbar}\left(\frac{\Omega_0}{\Omega_R}\right)^2 \frac{\Omega_R - \omega}{(\omega-\Omega_R)^2 + \Gamma^2},$$

$$\chi''_{zz}(\omega) = \frac{P_0}{\hbar}\left(\frac{\Omega_0}{\Omega_R}\right)^2 \frac{\Gamma}{(\omega-\Omega_R)^2 + \Gamma^2}, \tag{6}$$

where Γ denotes the dephasing rate for the transverse component of the Bloch vector to determine the qubit dynamics, the polarization constant $P_0=(\varepsilon/\Omega_R)\langle\hat{\sigma}_z\rangle$, $\langle\hat{\sigma}_z\rangle=\mathrm{Sp}\{\hat{\rho}\hat{\sigma}_z\}=1-2P_+$, $P_+ \le 0.5$ being the probability of the qubit excited state ($\hat{\rho}$ is the reduced density matrix of the qubit), at that $0 \le \langle\hat{\sigma}_z\rangle \le 1$. It is essential that the parameter P_0 and therefore $\chi''_{zz}(\omega)$ and the qubit-induced contribution to the effective damping rate of the tank $\bar{\gamma}_T$ [Eq. (3a)] alter their sign when the detuning parameter ε does so. Thus the effective resistance $\bar{R}_T \propto \bar{\gamma}_T$ contains a negative contribution R_q from the qubit at $\omega_g(\Phi_e) < n\omega_0 (\varepsilon<0, \bar{\gamma}_T < \gamma_T)$ and a positive contribution at $\omega_g(\Phi_e) > n\omega_0$ $(\varepsilon>0, \bar{\gamma}_T > \gamma_T)$.

As seen from Eq. (6), the functions $\chi'_{zz}(\omega), \chi''_{zz}(\omega)$ have nonmonotonous resonant character near n-photon Rabi frequencies. In their turn, as follows from Eq. (2), the weak continuous quantum measurement output functions V_T, α_T of the tank detector expressed through $\chi'_{zz}(\omega), \chi''_{zz}(\omega)$ have resonant contributions conditioned by coherent Rabi dynamics of the qubit at $\Omega_R \simeq \omega_T$ with small damping and decoherence rates $\Gamma < \Omega_R$. Notice that in previous spectroscopy experiments with charge-phase qubits,[31,32] there was only a small changing in the tank effective resistance [$\Gamma > \Omega_R$ and $\chi''_{zz}(\omega) \approx 0$, $\bar{R}_T \approx R_T$] and the voltage V_T conditioned by $\chi'_{zz}(\omega)$ could only decrease, as seen from Eq. (3c). In the case of coherent Rabi dynamics at $\Omega_R \approx \omega_T$, $\chi''_{zz}(\omega)$ can be nonzero while $\chi'_{zz}(\omega) \approx 0$, and the voltage V_T can both decrease or increase relative to the voltage level of the passive tank depending on the sign of $\chi''_{zz}(\omega_T) \propto R_q$.

Recently, the quantum theory of the low-frequency linear susceptibility of flux and charge-phase qubits subjected to microwave irradiation was developed within the density-matrix formalism in Ref. 19. This theory describes the parametric effects of reduction and amplification in signal and quality of the tank coupled to charge-phase qubits in the strong charge limit $E_{\mathrm{CP}} \gg \varepsilon_J(\pi)$.

The above theoretical outline gives only a qualitative picture of the effects in the system of charge-phase qubit and tank detector and cannot allow for their quantitative description. First, the charge-phase qubit has such parameters that $E_{\mathrm{CP}} \gtrsim \varepsilon_J(\pi)$ in our experiment, while its Hamiltonian and the energy spectrum are of more complicated structure as compared to the two-level approximation (1), and numerical solving of the Schrödinger equation is needed for this structure to be found. Another important feature is a strong nonlinearity of the qubit's response to the external electromagnetic excitation due to the Josephson character of the energy potential for the quantum coordinate of the system. As shown in the quantum-mechanical model of a SQUID ring coupled to an electromagnetic field,[40] the energy levels of the SQUID with coherent dynamics of magnetic flux change so dramatically in time when excited by strong electromagnetic field that their time averages essentially differ from the initial system levels. The shape of the time-averaged energy levels $\langle E_0 \rangle(\Phi_e)$ and $\langle E_1 \rangle(\Phi_e)$ in the high-power electromagnetic field depends on its frequency and amplitude in a compli-

cated manner, showing the compression between the levels and the interference patterns of resonant interactions between the two lowest ones. Similar by their nature effects are observed in nonlinear quantum optics. So, a two-level atom in strong electromagnetic field demonstrates nonlinear effects of the compression of its energy (quasi)levels and Stark effect.[41] Another basic aspect of the theoretical consideration of quantum dynamics of the qubit-detector system is taking into account the temperature effect resulting in finite width of the signal generation band in the qubit and in the tank, thus determining eventually the shape of the observed signal characteristics.

III. CHARGE-PHASE QUBIT AND EXPERIMENTAL RESULTS

A. Qubit calibration

The sample (see Fig. 1) was fabricated by electron-beam lithography and conventional two-angle technology of aluminum thin-film deposition to create two mesoscopic Josephson junctions with area $S_{J1,J2} \approx 3.5 \times 10^4$ nm^2, tunnel resistance $R_{J1,2} \approx 3.0$ kΩ, and $E_{J1,2}/h \approx 53$ GHz. The estimate of $R_{J1,2}$ was obtained from direct measurements of the tunnel resistance of a large-area "witness." Analysis of the scanning electron micrograph of the sample shows that the areas of the Josephson junctions in this charge-phase sample differ by approximately 15%. The difference between the areas of the junctions determines the asymmetry of the critical currents and leads to the optical evaluation of minimal value of the effective Josephson energy $\varepsilon_J(\pi)/h = |E_{J1} - E_{J2}|/h \approx 7$ GHz of the Cooper-pair transistor. The two-electron Coulomb energy evaluated on the basis of the geometric transistor capacitance is $E_{\mathrm{CP}}/h \approx 17$ GHz. The actual value of E_{CP} may be somewhat smaller due to the effect of the stray capacitance of the island. Thus, the two characteristic energies in the given qubit are on the same order of magnitude and meet the adiabaticity condition $\varepsilon_J(\pi) < E_{\mathrm{CP}} < \Delta_{\mathrm{Al}}(0)$.

Choosing $E_{\mathrm{CP}} \gtrsim \varepsilon_J(\pi)$ instead of the strong condition $E_{\mathrm{CP}} \gg \varepsilon_J(\pi)$, we decrease the influence of the nonequilibrium noise of the charge on coherent dynamics of the qubit.[2] For the same purpose,[29,42] both the ratio $(C_g/C_\Sigma)^2 \approx 2 \times 10^{-3}$ and the ratio of the real part of the charge-gate line impedance to the quantum resistance $\mathrm{Re}\, Z_g(\omega)/R_Q \approx 10^{-2}$ ($R_Q = h/4e^2$) are made small in the given sample of the charge-phase qubit. To reduce the qubit effective temperature T_{eff}, all the input electric circuits were thoroughly filtered by multiresonance (Cu)O powder filters, and the voltage supply resistor along with the last stage of the copper filter of the charge-gate line were placed onto 10 mK refrigerator stage for better thermalization.

The island volume allows us to estimate the number of states N_{eff} and the characteristic temperature[43] $T^* = \Delta_{\mathrm{Al}}(0)/k_B \ln N_{\mathrm{eff}} \approx 120$ mK, above which the number of the quasiparticle excitations in the island abruptly rises from zero.

The charge-phase qubit Hamiltonian (1) is sensitive to any changes in magnetic flux coupled to the superconducting loop. To minimize the external flux noise, the qubit superconducting loop is implemented as a first-order gradiometer with minimum distance between the coils. The achieved balancing accuracy (difference between the areas of the gradiometer coils) is on the order of one part in 10^3.

To read the change in the amplitude V_T and phase α_T of the oscillations, the tank circuit was linked to a preamplifier placed on 1-K-pot and room-temperature electronics. It should be emphasized that the part of the tank circuit kept at temperature $T \approx 1.7$ K (1 K pot) (see Fig. 1) is a source of high-frequency photons that can affect the qubit. Moreover, in addition to amplifying the in-band Rabi signal, it is obvious that the preamplifier can also irradiate at extremely high frequencies, thus increasing the effective temperature T_{eff} of the qubit. The qubit decoherence due to the backaction from both the tank circuit and the preamplifier depends on many parameters and was not analyzed yet in detail. We will return to this problem below. To reduce T_{eff}, the coupling coefficient was decreased to $k \approx 0.029\,5$ that led to the parameter $k^2 Q_0 \approx 0.3$. However, coupling to the tank circuit cannot be made arbitrarily small in Rabi qubit-based detectors for the purpose of reducing decoherence and should be optimized. We have found that $k^2 Q_0 \approx 0.3$ is close to the most optimal value that provides maximum (Rabi) signal-to-noise ratio due to the effect of high-frequency photons from the measuring circuit. This value substantially differs from the usual match condition $k^2 Q_0 \gtrsim 1$ for classic rf SQUIDs.[16,33,34] Despite the fact that the main part of the tank circuit is placed at $T \approx 10$ mK, its effective noise temperature $T_T^N \approx 400$ mK in our experiments. It can be shown[17,29] that at $\Omega_R = \omega_T$, the tank with impedance $\omega_T L_T Q_0 = (11.34 \pm 0.02)$ kΩ at mutual inductance $M = k\sqrt{L_T L_q} = (0.365 \pm 0.005)$ nH in the band $\gamma_T = 85$ kHz contributes sufficiently small noise flux $\Phi_T^N \approx 2 \times 10^{-6} \Phi_0$ to the qubit outside the region of the exact resonance.

The previous measurements showed that superfluous noises from the microwave line at galvanic coupling with a qubit were unavoidable. Therefore, all experimental results were obtained with the qubit placed in a Pb resonator in the region of maximum electric field. The qubit was then continuously irradiated with a microwave field to introduce an alternating voltage component $V_r \cos \omega_0 t$. So, the capacitance C_E formally galvanicly coupled to the charge-gate capacitance C_g in Fig. 1 denotes—in fact—coupling of the qubit charge gate to a microwave field. Since the distribution of the electric field only approximately corresponds to that expected for an ideal resonator, we made preliminary measurements of the qubit response to the microwave field as a function of its frequency in the range of 6.6–8.0 GHz.

A detailed analysis of the qubit dynamics has shown that extremal positive (peak) and negative (dip) responses $V_T(\Phi_e)$ to low-amplitude microwave field were observed at frequency $f \equiv \omega_0/2\pi \cong 7.27$ GHz, with small deviations $0.010\Phi_0$ and $0.017\Phi_0$ from the point $\Phi_e = 0.5\Phi_0$. Assuming that the single-photon process of the higher-level excitation occurs at frequency $f = 7.27$ GHz, we find the effective Josephson energy $\varepsilon_J(\pi)/h \approx 6.4$ GHz.

B. Single-photon Rabi response

Assuming that one should observe the resonant parametric response of the qubit in the region of Rabi frequencies

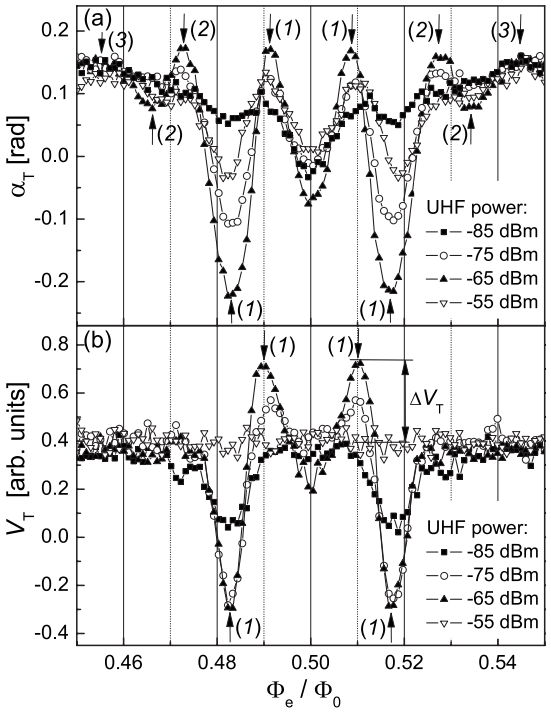

FIG. 2. Experimental results for the charge-phase qubit placed in the region of the maximum electric field under continuous microwave irradiation with $f=7.27$ GHz. (a) Set of the curves of the voltage-current phase shift $\alpha_T(\Phi_e/\Phi_0)$ in the tank circuit; (b) set of the curves of the amplitude of the voltage oscillations $V_T(\Phi_e/\Phi_0)$ in the tank circuit. The curves parameter is the microwave power. The arrows denote extrema of $\alpha_T(\Phi_e/\Phi_0)$ and $V_T(\Phi_e/\Phi_0)$ for single-, two-, and three-photon excitations. The signal shape near resonances is determined by the finite width of the Rabi generation band. The maximum response is observed at $P \approx -65$ dBm.

$\Omega_R \simeq \omega_T$ when the microwave field frequency was near that of single-photon transitions, we investigated in detail dependencies $V_T(\Phi_e)$ and $\alpha_T(\Phi_e)$ at various amplitudes (powers) of the microwave field. Typical measurement results at $f=7.27$ GHz are shown in Figs. 2(a) and 2(b). It is clearly seen from these curves that the single-photon resonant response predicted by Eqs. (3)–(6) and smeared out by the temperature noise and coupling to the readout device is observed at an optimal microwave power. Change in the shape of the dependence $V_T(\Phi_e)$, $\Delta V_T \propto -\mathrm{Re}\, Z(\omega)$, due to the resistance $\mathrm{Re}\, Z(\omega)$ inserted from the qubit into the tank, allows us to distinguish the following regions $\omega_g(\Phi_e) < \omega_0$, $\omega_g(\Phi_e) = \omega_0$, $\omega_g(\Phi_e) > \omega_0$, for which the inserted resistance take the following values $\mathrm{Re}\, Z(\omega) < 0$, $\mathrm{Re}\, Z(\omega) = 0$, and $\mathrm{Re}\, Z(\omega) > 0$, respectively. In the region $\omega_g(\Phi_e) < \omega_0$, the negative resistance is inserted into the tank and its quality increases due to the transferring energy from the qubit to the tank. At resonant condition $\omega_g(\Phi_e) = \omega_0$, the tank energy is kept constant on average, and in the region $\omega_g(\Phi_e) > \omega_0$, energy is transferred in the counter direction from the tank to the qubit and the tank quality factor decreases. In Figs. 2(a) and 2(b), the extrema of the dependencies $V_T(\Phi_e)\alpha_T(\Phi_e)$ arising due to single-, two-, and three-photon resonant excitations are labeled by arrows enumerated according to the resonance number. Each region of the resonant excitation is characterized by the "peak" and "dip" extrema points Φ_e to the left and to the right of the point of strict resonance for $\Phi_e > 0.5\Phi_0$ (and vice versa for $\Phi_e < 0.5\Phi_0$), at which the maximum negative or positive resistance is inserted from the qubit into the tank circuit. The decrease, as well as increase, in the microwave power compared to its optimal value results in falling of the resonant response amplitude that is explained by the rise of the detuning $\xi = \Omega_R(V_r) - \omega_T$.

The variations $V_T(\Phi_e), \alpha_T(\Phi_e)$ in these experiments are measured simultaneously and, since the rf generator frequency is chosen from the condition $\omega_{\mathrm{rf}} \cong \omega_T$, the technique sensitivity is maximal with respect to the change in the oscillations phase. On the contrary, sensitivity of the voltage channel to small changes in the resonant frequency of the tank ω_T near $\omega_T \approx \omega_{\mathrm{rf}}$ is minimal. Notice the two-photon resonant response seen fairly well in $\alpha_T(\Phi_e)$ curves in the vicinity of $\Phi_e = 0.53\Phi_0$ [Fig. 2(a)], whereas having signal-to-noise ratio $S/N \approx 1$ at $V_T(\Phi_e)$ characteristics. The decrease in the amplitude of the two-photon resonant response relative to the single-photon one in Fig. 2(a) agrees with the theory[17] that predicts the longest decoherence time in the point of symmetry $\Phi_e = 0.5\Phi_0$.

In the general case, variations in the phase as well as the amplitude of the parametric oscillations in the tank circuit are bounded to the change in its resonance frequency and quality. Thus, the dependencies $\alpha_T(\Phi_e)$ and $V_T(\Phi_e)$ presented in Figs. 2(a) and 2(b) qualitatively confirm the existence of the low-frequency part of the charge-phase qubit susceptibility function (6) as the Rabi frequency Ω_R of the qubit passes through the resonant frequency ω_T of the tank. Let us consider the evolution of the signals V_T in vicinity of the point $\delta = \pi$. As it follows from the expression (3), the Rabi response of the qubit in the point $\delta = \pi$ should vanish proportionally to the square of the circulating current I_q^2. At low amplitudes of the microwave field, the responses V_T are really small as it is seen from Fig. 2(b). However, at power $P = -65$ dBm noticeable shifts ΔV_T (as well as $\Delta \alpha_T$) are observed which signifies the appearance of circulating current in the point $\delta = \pi$ at the expense of deviation of time-averaged eigenenergies from stationary eigenenergies.[40]

We use the noise spectroscopy method for the direct impedance measurements. In this case, the generator current $I_{\mathrm{rf}} = 0$ and the tank circuit is excited by thermodynamic fluctuations, while its characteristics depend on the impedance inserted from the qubit under continuous irradiation. Figure 3 displays the noise spectral density as a function of frequency for the two extreme (peak and dip) points denoted by arrows in Fig. 2(b) and at the degeneracy point $\delta = \pi$. It is seen from these amplitude-frequency characteristics measured at minimal influence of the tank circuit on the qubit that Rabi oscillations result in a visible change in the tank quality and a shift of the tank resonant frequency in the peak and dip Φ_e points (curves and in Fig. 3, respectively). As discussed above, the sign of the Rabi impedance inserted from the qubit is determined by the sign of the detuning $\varepsilon = \omega_g(\Phi_e) - \omega_0$ between the energy gap $\omega_g(\Phi_e)$ and microwave field frequency ω_0. From the quality factor values and the resonant frequencies in the extreme points indicated in Fig. 3 and using Eq. (4), we deduce that the maximum value of the negative resistance inserted into the tank $R_q = R^{\mathrm{peak}} \approx$

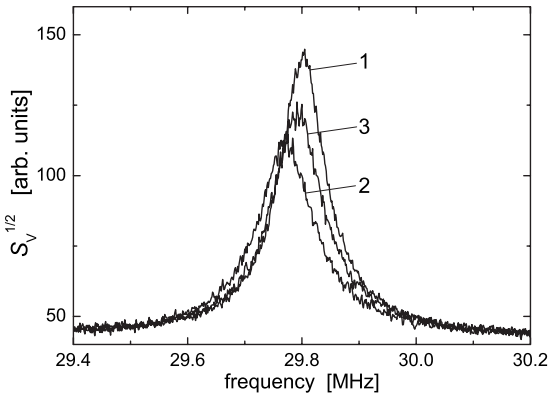

FIG. 3. Noise spectroscopy of the tank circuit obtained for the charge-phase qubit, being under microwave irradiation with frequency $f=7.27$ GHz. Set of curves of the noise spectral density of the tank circuit as a function of frequency obtained at optimal microwave power ($P\approx -65$ dBm) in extreme points 1 $\Phi_e^{\text{peak}} \approx 0.49\Phi_0, 0.51\Phi_0$ ($Q^{\text{peak}} \approx 360$), 2 $\Phi_e^{\text{dip}} \approx 0.483\Phi_0, 0.517\Phi_0$ ($Q^{\text{dip}} \approx 258$), and in the degeneracy point 3 $\Phi_e \approx 0.5\Phi_0$ ($Q \approx 301$). The resonant frequencies $\omega_T/2\pi$ in these points are 29.803, 29.770, and 29.795 MHz, respectively.

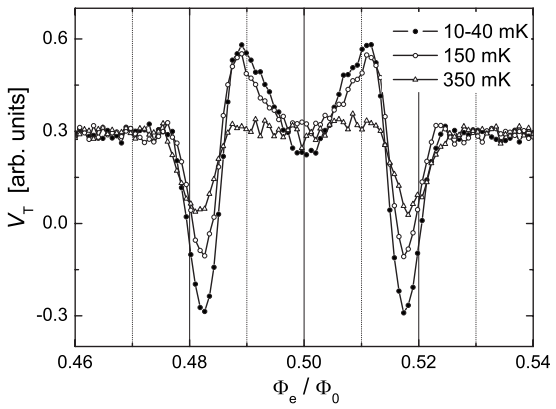

FIG. 4. Set of curves $V_T(\Phi_e/\Phi_0)$ obtained under microwave irradiation with frequency $f=7.27$ GHz. The microwave field amplitude is optimal for each curve. The curve parameter is the refrigerator temperature (measured with an estimated accuracy 5 mK).

$-0.017\,3\ \Omega$ practically coincides with the maximum positive resistance $R^{\text{dip}} \approx 0.017\,6\ \Omega$ by the absolute magnitude, while the alteration of its sign implies the transition from the irradiation to the absorption properties of the qubit. The inductance contributions in these points are small ($L_q^{\text{peak}} \approx -0.53\times 10^{-3} L_T$, $L_q^{\text{dip}} \approx 1.68\times 10^{-3} L_T$) and are also of opposite signs. Variation in the quality factor between the extreme points relative to the quality in the degeneracy point amounts to the appreciable value $(Q^{\text{peak}} - Q^{\text{dip}})/Q \approx 34\%$.

Note that similar electrodynamics is typical for the parametric interaction of a resonator microwave signal with Josephson oscillations.[14–16] In this classic analog, the maximum amplitude of the parametric effect is determined by fluctuations of the average junction voltage that lead to broadening of the Josephson generation band. So, assuming that the rise of the qubit temperature in the considered case of Rabi oscillations will result in broadening of their spectrum, one should expect some decrease in the amplitude of the inserted negative impedance with increasing the bath temperature.

The analysis of temperature dependencies demonstrates that the amplitude of the inserted resistances $R^{\text{peak}}, R^{\text{dip}}$ within experimental accuracy does not depend on T_{bath} in the interval $T_{\text{bath}}=10-40$ mK. The amplitude of the inserted impedance decreased by 15% at $T_{\text{bath}}=60$ mK and the extrema in curves $V_T(\Phi_e/\Phi_0)$ smooth out in the interval 60–100 mK. The increase in the bath temperature up to 150–200 mK leads to the dramatic fall of the amplitude ΔV_T. Note that the calculated temperature $T^* \cong 120$ mK, at which abrupt decay of the coherent effects is expected, is close to the experimental data. The coherence degradation at $T > T^*$ is accompanied by fast shortening of the decoherence time and widening of the Rabi oscillation band. Further, temperature T_{bath} rise up to 300–350 mK causes the Rabi impedance of the qubit seen by the tank to vanish ($\Delta V_T = 0$) within the noise level, i.e., the coherent Rabi effects disappear.

The minimal effective temperature of the qubit estimated to be $T_{\text{eff}}=(80\pm 10)$ mK is determined mainly by the effect of the readout circuit [tank detector and high electron mobility transistor (HEMT) amplifier] and leads to sufficiently large uncertainty in the magnetic flux $\delta\Phi=(k_B L_q T_{\text{eff}})^{1/2} \approx 0.01\Phi_0$ for the qubit under consideration. Anyway, the dependence Re $Z(\omega) \propto \chi''_{zz}(\omega)$ on the microwave power and the temperature indicates the presence of coherent quantum oscillations at low temperatures that have potential applications as a self-Rabi pumping signal in quantum information detectors.

It is seen from the results presented in Fig. 4 that at the bath temperature 350 mK near $\Phi_e^{\text{dip}} \approx 0.483\Phi_0, 0.517\Phi_0$, the dips are still observed and are associated with the processes of noncoherent quantum tunneling of Cooper pairs, without forming a superposition of the charge states. Therefore, the contribution of the coherent oscillations in the given temperature interval is described as the difference between the values of $V_T(\Phi_e)$ obtained at 10 and 350 mK. Taking into account that the presence of the coherent oscillations at optimal amplitude of the microwave field leads to a 17% change in the tank quality, the evaluation can be made at our parameters for the minimum decoherence time $\tau_\varphi^{\min} > 2\pi/\omega_T \approx 0.033$ μs. While the charge-flux qubit is an ideal frequency downshifter, one can evaluate τ_φ from the high-frequency resonance linewidth that yields three times as large values of $\tau_\varphi \approx 0.1$ μs.

According to the theory,[41] the enhancement of Q_q is possible not only at the expense of lowering the noise temperatures of the qubit and the tank but also due to narrowing of the n-photon resonance band when going to the region of the multiphoton Rabi oscillations. The evidence of the two- and three-photon resonances in a similar charge-phase qubit was demonstrated in the previous work.[32]

C. Multiphoton Rabi response

It follows[41] from the theory of two-lewel atom in strong low-frequency electromagnetic field that the quality of the multiphoton resonance considerably rises, while the reso-

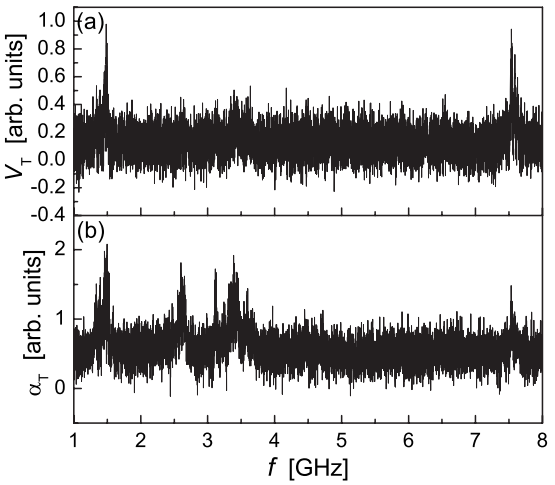

FIG. 5. Resonant excitation of the charge-phase qubit. Amplitude $V_T(f)$ and phase $\alpha_T(f)$ of the tank circuit oscillations ($MI_T < 10^{-4}\Phi_0$, $\omega_{\rm rf} \approx \omega_T$) vs the frequency of the microwave field in the charge gate of the charge-phase qubit with $n_g \approx 1$, $\delta \approx \pi$. The $1/f$ noise level becomes important because of the long-continued (4 h) spectrum registration. Multiphoton resonance from the ground state to the first-excited state induced by the photon frequency $f \approx 1.4$ GHz is clearly seen. The generator microwave field amplitude is kept constant $P=-60$ dBm when frequency sweeping; the bath temperature being 10mK.

nance order grows owing to the coherent addition of individual transition amplitudes. The narrowing of distribution of the excited level occupation probability must result in a natural filtration of noise photons in the above-discussed effect of the interaction between the tank circuit current and the Rabi-type oscillations in the charge-phase qubit. At the same time, the amplitude of the synchronization effect causing the energy irradiation (absorption) by the qubit at frequencies close to that of the multiphoton Rabi oscillations may increase. In other words, the signal characteristics, the conversion steepness, and the sensibility of a parametric detector based on the charge-phase qubit must enhance when coming to the multiphoton excitation. Depending on the interplay between quantities included in Hamiltonian (1), such a detector could be sensitive to the induced charge such as rf single-electron transistor detector[44] and to the magnetic flux such as SQUIDs (Refs. 33 and 34) and detectors based on the flux qubit.[45]

During the multiphoton experiments, the parameters of the charge-phase qubit, its position inside the resonator, and the measuring circuitry (Fig. 1) to detect the response by the technique of weak continuous measurement remained the same, as in "single-photon" measurements described in the previous section.

Spectroscopic studies were performed in wide (1–8 GHz) frequency range to find the frequencies of the multiphoton resonances of the charge-phase qubit ($n_g \approx 1$, $\delta \approx \pi$) (see Fig. 5). At sweeping the frequency of the small-amplitude microwave field, the time-averaged upper-level occupation probability goes through a pronounced maximum at frequency values meeting the exact multiphoton resonance condition[46] that leads to the maximum qubit response. However, the effectiveness of excitation of the multiphoton resonance depends on the generator power and the distribution of the field in the resonator. So, if for a certain frequency of the multiphoton resonance the charge-phase qubit is situated in a peak (a node) of the electrical field then the amplitude $V_r \cos \omega_0 t$ at the charge gate reaches its maximum (minimum). As seen from Fig. 5(b), in our experiments good excitation conditions occurred for single-, two-, three-, and five-photon resonances; while from Fig. 5(a) it is seen that the resonant parametric interaction of the qubit and the tank circuit occurred at single- and five-photon resonances.

Therefore, we concentrated on the experimental study of the five-photon resonance excited at a frequency close to 1.4 GHz (7.27 GHz/1.4 GHz ≈ 5). Note that the microwave generator-to-resonator and resonator-to-qubit transmission lines have their own resonances (frequency-dependent coupling between the MW generator and qubit). This evokes a nonmonotonic frequency dependence of the injected microwave power and, with taking into account the nonlinear transformation in the qubit, to the appearance of additional spectral lines. Noticeable spread in the peaks positions along the frequency axis and excessive peak width in Fig. 5 is associated with a drift of the qubit parameters ($1/f$ noise) because of the long-lasting ($\sim$4 h) frequency sweeping. Therefore, at the next stage, analyzing the qubit response $\alpha_T(f)$ to the microwave field in a narrow frequency band, we have found that the resonant frequency for the five-photon transition was close to $f=1.444$ GHz.

To determine the effective width of the resonance line (quality factor), two series of measurements were performed for the phase of oscillations in the tank circuit as a function of the magnetic flux applied to the qubit and the microwave field parameters (i) $\alpha_T(\delta)$ at a fixed microwave field amplitude V_r for several frequencies near $f=1.444$ GHz and (ii) $\alpha_T(\delta)$ at the resonant frequency $f=1.444$ GHz for several microwave field amplitudes. Typical results for the measurements of the series (i) and (ii) are shown in Figs. 6 and 7, respectively. Since maximum detuning of the microwave generator from the resonance for the set presented in Fig. 6 is small ($\Delta\omega_0/\omega_0 \cong 0.014$), the power in the channel can be considered as being practically constant while sharp dependence of the $\alpha_T(\delta)$ shape on the microwave field frequency should be associated with the quality of the five-photon resonance. It follows from the comparison between the series of the measurements (i) and (ii) that the drop in the microwave field power by 2 dB at fixed frequency $f=1.444$ GHz [couple of curves in Figs. 7(a) and 7(b)] results practically in the same transformation of the $\alpha_T(\delta)$ shape as when the microwave field frequency changes from $f=1.444$ to 1.460 GHz or to 1.435 GHz at a fixed generator power (couple of curves in Figs. 6(c) and 6(a) or Figs. 6(c) and 6(e), respectively). Therefore, the effective quality of the five-photon resonance in the charge-phase qubit reaches $Q_{n=5} = 1.444/(1.460-1.435) = (58 \pm 5)$ at 2 dB change in the microwave power. Taking the two shape-alike dependences at positive [Fig. 6(b)] and negative [Fig. 6(d)] detunings and assuming that the population at a multiphoton resonance is almost symmetric with respect to the detuning sign, we will have for the resonance frequency $f=(1.440+1.450)/2 \approx 1.445$ GHz that is close to the value determined earlier.

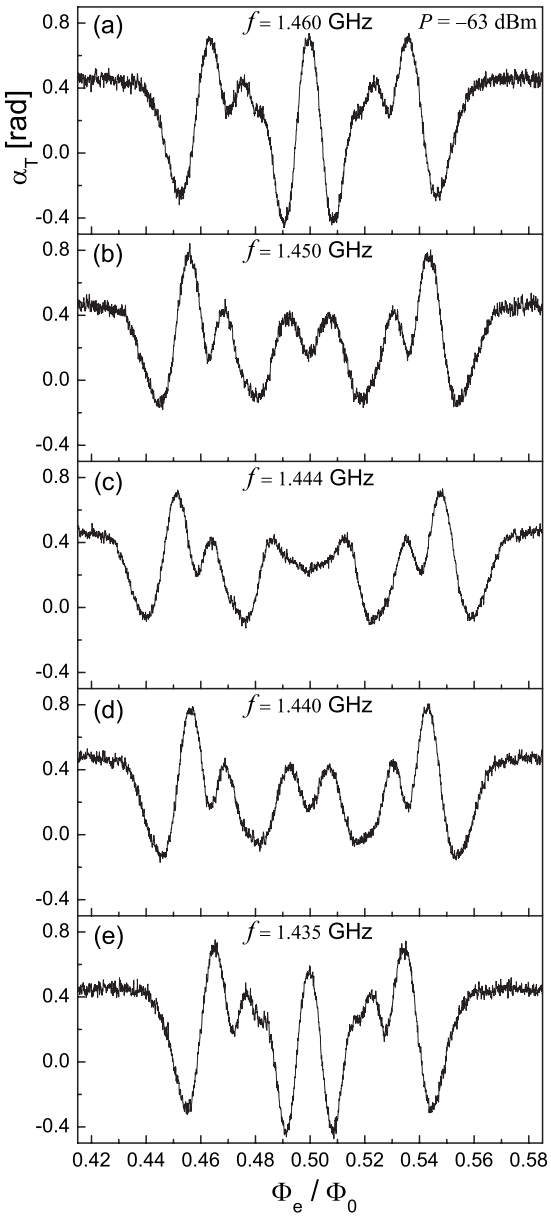

FIG. 6. Set of signal characteristics $\alpha_T(\Phi_e/\Phi_0)$ of charge-phase qubit in the microwave field in the vicinity of the five-photon resonance at the bath temperature of 10 mK. The curves parameter is the microwave frequency. The generator power $P=-63$ dBm is kept constant for all the curves. The characteristics set (a)–(e) reflects the dependence of the probability excitation on the frequency at (a) positive, [(b) and (d)] and negative, (e) detuning relative to the resonance frequency (c) $f=1.444$ GHz.

Owing to the high effective quality of the five-photon resonance, the response of the charge-phase qubit to the charge variation considerably increases as compared to the case of the single-photon excitation. As it is seen from Fig. 8, the change in the polarization charge by $\Delta n_g \approx 1$ causes $\Delta\delta \approx 0.01\pi$ shift of the peaks and dips associated with the qubit's functions $\chi'(\omega), \chi''(\omega)$. For the single-photon Rabi response, we get the values which are five times as little. Typical amplitudes of change of α_T in the five-photon experiment is almost a factor of 5 as compared to single-photon measurements, giving an estimate for the minimum decoherence time of the five-photon Rabi oscillations $\tau_\varphi=0.17$ μs. This confirms the above assumption about the lesser effect of noise in the region of the multiphoton resonances. In connec-

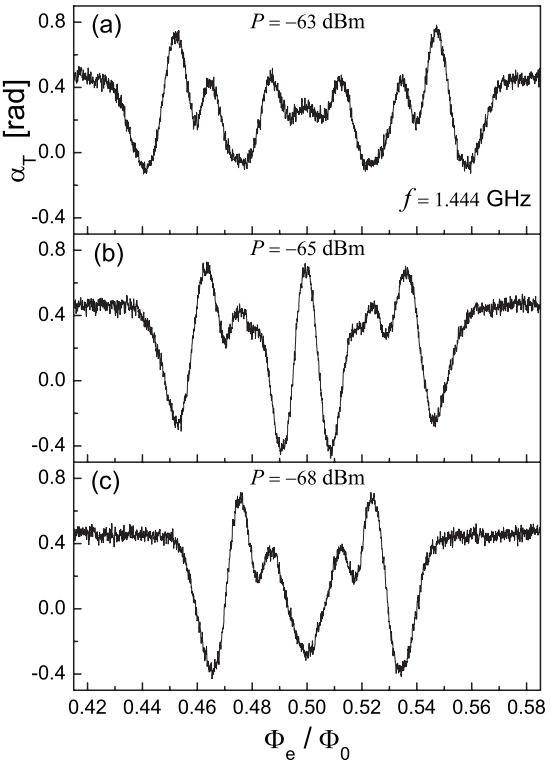

FIG. 7. Set of signal characteristics $\alpha_T(\Phi_e/\Phi_0)$ of charge-phase qubit in microwave field with frequency $f=1.444$ GHz. The curves parameter is the microwave power. It is well seen that the dependence taken at $P=-65$ dBm practically coincides with the curves obtained at $P=-63$ dBm and at frequencies 1.460 and 1.435 GHz [see Figs. 6(a) and 6(e)].

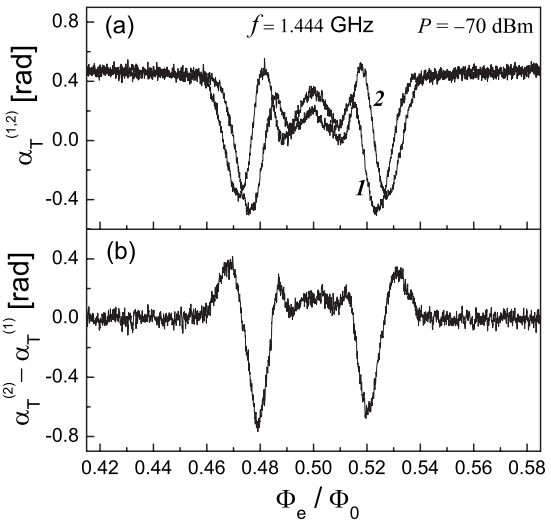

FIG. 8. (a) Signal characteristics $\alpha_T^{(1,2)}(\Phi_e/\Phi_0)$ of charge-phase qubit in microwave field ($P=-70$ dBm, $f=1.444$ GHz) for two values: (1) $n_g \approx 1$ and (2) $n_g \approx 0$ in the charge gate. (b) The signal difference $\alpha_T^{(2)} - \alpha_T^{(1)}$ for the change $\Delta n_g = n_g^{(1)} - n_g^{(2)} \approx 1$.

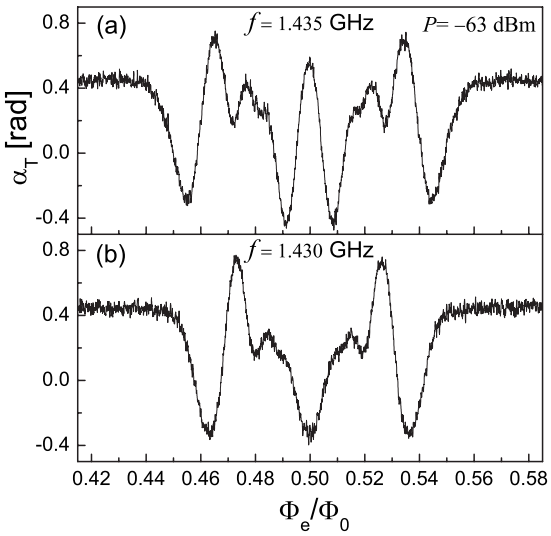

FIG. 9. Interference-induced variation in signal characteristics $\alpha_T(\Phi_e/\Phi_0)$ of the charge-phase qubit at the symmetry point $\Phi_e = 0.5\Phi_0$. Maximum $\alpha_T(0.5\Phi_0) \approx 0.5$ (a) transforms into minimum $\alpha_T(0.5\Phi_0) \approx -0.4$ (b) when the microwave frequency is detuned by $\Delta f = 5$ MHz ($\Delta f/f = 0.0035$) at fixed microwave generator power $P = -63$ dBm.

tion with this, it should be noted that the measurement of the charging energy E_{CP} of Hamiltonian (1) of a charge-phase qubit in the single-photon resonance mode may bring up considerably overestimated total capacitance of the island C_Σ because of the charge-gate noise.

The characteristic behavior of $\alpha_T(\delta)$ shown in Figs. 6–8 indicates that if the qubit is excited at frequencies close to those of the five-photon resonance then peaks and dips are observed (such as in the case of the single-photon excitation) and caused by the alteration of sign of the Rabi impedance inserted in the tank circuit when crossing the resonance region $n\hbar\omega_0 \cong \Delta E(\delta, n_g)$. The increase in the tank circuit quality observed at the single- and five-photon excitations reflects the fact that the microwave field energy being transformed by the qubit into Rabi-type oscillations is transferred to the tank circuit. The decrease in the quality corresponds to the reverse energy flow.

The interference character of the interaction between the microwave field with frequency ω_0 and the time-dependent frequency equivalent energy gap $\omega_g(\delta, n_g)$ of the charge-phase qubit leads to a sharp dependence of the shape of the signal characteristics of the qubit detector on the microwave field parameters. An example of such a dependence which emphasizes high sensitivity of the multiphoton spectroscopy is shown in Fig. 9. In this case, the peak observed at $\delta = \pi$ and frequency $f = 1.435$ GHz transforms into a dip with shifting the frequency of the microwave field by 5 MHZ, i.e., $\Delta f/f \approx 3.5 \times 10^{-3}$.

Observed quasiperiodicity of the signal characteristics $\alpha_T(\delta)$, $V_T(\delta)$ of the charge-phase qubit (see Figs. 6 and 7) is determined by the behavior of the quasienergy (qubit's macrolevels) population in the magnetic and electromagnetic fields. The rise of $\varepsilon_J(\delta)$ at the deviation of the external magnetic flux from $0.5\Phi_0$ leads to meeting the resonant conditions for resonances of higher order, and the time-averaged upper-level occupation probability reaches its maximum. If the microwave power is such that the frequency of the excited multiphoton Rabi oscillations is close to the tank circuit frequency, the interaction between the Rabi oscillations with the tank circuit oscillations will turn again to the parametric increase (decrease) in the signals. The typical period of such dependence on the magnetic flux is determined by the qubit's energy gap $\Delta E(\Phi_e)$ as a function of the magnetic flux.

IV. CONCLUSIONS

We have described experiments which demonstrated the coherent Rabi-type oscillations in a charge-phase qubit being under continuous microwave irradiation, involving single- and multiphoton quantum dynamics in the state of weak coupling to a radio-frequency tank detector. Our results show that the charge-phase qubit appears to be quite sensitive as a quantum parametric detector with self-pumping provided by the inner Rabi generation (Figs. 2 and 6–9). In the first series of experiments, we measured the magnetic-flux dependence of the qubit response, the qubit being irradiated by the microwave field with frequencies in the region of the single-photon transitions (Fig. 2). It was shown by the noise spectroscopy that the extrema appearing in the signal characteristics $\alpha_T(\Phi_e/\Phi_0)$ and $V_T(\Phi_e/\Phi_0)$ were mainly due to the increase and decrease in the tank circuit quality and reflected the fact that the power in these (corresponding to the extrema) points flowed from the microwave field into the tank circuit (peaks) and vice versa (dips) (Fig. 3). With the microwave power at its optimum value to provide the maximum response, we observed that the resistance Re $Z(\omega)$ inserted from the qubit into the tank circuit at the extrema points rapidly fell in the region $T \approx 150$–200 mK approaching to zero in 250–350 mK region within the experimental uncertainties (Fig. 4). We believe that the effective noise temperature of the qubit $T_{\mathrm{eff}} \approx 80$ mK and the decoherence rate in our experiments are determined by the irradiation from the part of the tank circuit and the transistor placed at $T \approx 1.7$ K. The development of an improved type of readout with small backaction effect would be a major step forward for further improving characteristics of the qubit detector with self-pumping by intrinsic Rabi generation. At the same time, the extension of theory to nonzero temperatures would be of great significance for understanding the temperature effect on the coherent quantum phenomena in qubits[47] and conditioned by them detected signals. In the second series of the experiments, we measured the qubit response to the variation in the magnetic flux and the electric charge in microwave field near the five-photon resonance (Figs. 6–9). An enhancement of the quality of the multiphoton resonances, as it was supposed according to the theory,[41] results in the partial filtration of noise photons and the increase in amplitude of the signal characteristics of the detector associated with the multiphoton Rabi oscillations. The fact that the high transducing steepness is observed at the point $\delta = \pi$ for some signal characteristics $\alpha_T(\delta)$ in the region of five-photon resonance points out to a sharp dependence of quasienergy on microwave power and, hence, to a strong nonlinearity of the system at high powers.[40]

ACKNOWLEDGMENTS

The authors would like to thank A. Izmalkov, Th. Wagner, S.V. Kuplevakhsky, S.N. Shevchenko, and O. G. Turutanov for helpful discussions. The work was partially supported by the Deutsche Forschungsgemeinschaft under Contract No. KR1172/9-2 and within the Nanophysics and nanoelectronics" program of the Ministry of Education and Science of Ukraine under Grant No. M/189-2007.

*shnyrkov@ilt.kharkov.ua

†Present address: Institute of Photonic Technology, P.O. Box 100239, D-07702 Jena, Germany.

[1] Y. Nakamura, Yu. A. Pashkin, and J. S. Tsai, Phys. Rev. Lett. **87**, 246601 (2001).

[2] D. Vion, A. Aassime, A. Cottet, P. Jooyez, H. Pothier, C. Urbina, D. Esteve, and M. H. Devoret, Science **296**, 886 (2002).

[3] I. Chiorescu, Y. Nakamura, C. J. P. M. Harmans, and J. E. Mooij, Science **299**, 1869 (2003).

[4] J. M. Martinis, S. Nam, J. Aumentado, and C. Urbina, Phys. Rev. Lett. **89**, 117901 (2002).

[5] S. Saito, M. Thorwart, H. Tanaka, M. Ueda, H. Nakano, K. Semba, and H. Takayanagi, Phys. Rev. Lett. **93**, 037001 (2004).

[6] S. Saito, T. Meno, M. Ueda, H. Tanaka, K. Semba, and H. Takayanagi, Phys. Rev. Lett. **96**, 107001 (2006).

[7] M. B. Metcalfe, E. Boaknin, V. Manucharyan, R. Vijay, I. Siddiqi, C. Rigetti, L. Frunzio, R. J. Schoelkopf, and M. H. Devoret, Phys. Rev. B **76**, 174516 (2007).

[8] J. Clarke and K. Wilhelm, Nature (London) **453**, 1031 (2008).

[9] R. F. Voss and R. A. Webb, Phys. Rev. Lett. **47**, 265 (1981).

[10] J. M. Martinis, M. H. Devoret, and J. Clarke, Phys. Rev. B **35**, 4682 (1987).

[11] I. M. Dmitrenko, V. A. Khlus, G. M. Tsoi, and V. I. Shnyrkov, J. Low Temp. Phys. **11**, 77 (1985).

[12] A. J. Leggett, Prog. Theor. Phys. **69**, 80 (1980).

[13] J. R. Friedman, V. Patel, W. Chen, S. K. Tolpygo, and J. E. Lukens, Nature (London) **406**, 43 (2000).

[14] H. Kanter and F. L. Vernon, Jr., J. Appl. Phys. **43**, 3174 (1972).

[15] A. N. Vystavkin, V. N. Gubankov, L. S. Kuz'min, K. K. Likharev, V. V. Migulin, and A. N. Spitsyn, JETP Lett. **17**, 284 (1973).

[16] K. K. Likharev, *Dynamics of Josephson Junctions and Circuits* (Gordon & Breach, Amsterdam, 1986).

[17] A. Yu. Smirnov, Phys. Rev. B **68**, 134514 (2003).

[18] W. Krech, D. Born, V. Shnyrkov, Th. Wagner, M. Grajcar, E. Il'ichev, H.-G. Meyer, and Y. Greenberg, IEEE Trans. Appl. Supercond. **15**, 876 (2005).

[19] Ya. S. Greenberg and E. Il'ichev, Phys. Rev. B **77**, 094513 (2008).

[20] J. Hauss, A. Fedorov, C. Hutter, A. Shnirman, and Gerd Schön, Phys. Rev. Lett. **100**, 037003 (2008).

[21] M. Grajcar, S. H. W. van der Ploeg, A. Izmalkov, E. Il'ichev, H.-G. Meyer, A. Fedorov, A. Shnirman, and Gerd Schön, Nat. Phys. **4**, 612 (2008).

[22] A. Izmalkov, S. H. W. van der Ploeg, S. N. Shevchenko, M. Grajcar, E. Il'ichev, U. Hübner, A. N. Omelyanchouk, and H.-G. Meyer, Phys. Rev. Lett. **101**, 017003 (2008).

[23] S. N. Shevchenko, S. H. W. van der Ploeg, M. Grajcar, E. Il'ichev, A. N. Omelyanchouk, and H.-G. Meyer, Phys. Rev. B **78**, 174527 (2008).

[24] D. Vion, P. F. Orfila, P. Joyez, D. Esteve, and M. H. Devoret, J. Appl. Phys. **77**, 2519 (1995).

[25] N. Grønbech-Jensen and M. Cirillo, Phys. Rev. Lett. **95**, 067001 (2005).

[26] A. B. Zorin, Physica C **368**, 284 (2002).

[27] W. Krech, M. Grajcar, D. Born, I. Zhilyaev, Th. Wagner, E. Il'chev, and Ya. Greenberg, Phys. Lett. A **303**, 352 (2002).

[28] J. R. Friedman and D. V. Averin, Phys. Rev. Lett. **88**, 050403 (2002).

[29] A. B. Zorin, J. Exp. Theor. Phys. **125**, 1423 (2004).

[30] M. Tinkham, *Introduction to Superconductivity*, 2nd ed. (McGraw-Hill, New York, 1996), Chap. 7; D. V. Averin and K. K. Likharev, in *Mesoscopic Phenomena in Solids*, edited by B. L. Altshuler, P. A. Lee, and R. A. Webb (Elsevier, Amsterdam, 1991), p. 173.

[31] D. Born, V. I. Shnyrkov, W. Krech, Th. Wagner, E. Il'ichev, M. Grajcar, U. Hübner, and H.-G. Meyer, Phys. Rev. B **70**, 180501(R) (2004).

[32] V. I. Shnyrkov, Th. Wagner, D. Born, S. N. Shevchenko, W. Krech, A. N. Omelyanchouk, E. Il'ichev, and H.-G. Meyer, Phys. Rev. B **73**, 024506 (2006).

[33] R. Rifkin, D. A. Vincent, B. S. Deaver, and P. K. Hansma, J. Appl. Phys. **47**, 2645 (1976).

[34] V. I. Shnyrkov, V. A. Khlus, and G. M. Tsoi, J. Low Temp. Phys. **39**, 477 (1980).

[35] A. N. Korotkov and D. V. Averin, Phys. Rev. B **64**, 165310 (2001).

[36] D. V. Averin, in *Exploring the Quantum/Classical Frontier: Recent Advance in Macroscopic Quantum Phenomena*, edited by J. R. Frirdman and S. Han (Nova, Hauppauge, NY, 2002), p. 441.

[37] E. Il'ichev, N. Oukhanski, A. Izmalkov, Th. Wagner, M. Grajcar, H.-G. Meyer, A. Yu. Smirnov, A. Maassen van den Brink, M. H. S. Amin, and A. M. Zagoskin, Phys. Rev. Lett. **91**, 097906 (2003).

[38] M. Sillanpää, T. Lehtinen, A. Paila, Y. Makhlin, and P. Hakonen, Phys. Rev. Lett. **96**, 187002 (2006).

[39] E. M. Lifshitz and L. D. Landau, *Statistical Physics: Course of Theoretical Physics*, 3rd ed. (Butterworth, London, 1984), Vol. 5, Chap. 12, p. 377.

[40] M. J. Everitt, P. Stiffell, T. D. Clark, A. Vourdas, J. F. Ralph, H. Prance, and R. J. Prance, Phys. Rev. B **63**, 144530 (2001).

[41] V. P. Krainov and V. P. Yakovlev, Sov. Phys. JETP **51**, 1104 (1980).

[42] Y. Makhlin, G. Schön, and A. Shnirman, Rev. Mod. Phys. **73**, 357 (2001).

[43] M. T. Tuominen, J. M. Hergenrother, T. S. Tighe, and M. Tinkham, Phys. Rev. Lett. **69**, 1997 (1992).

[44] R. J. Schoelkopf, P. Wahlgren, A. A. Kozhevnikov, P. Delsing, and D. E. Prober, Science **280**, 1238 (1998).

[45] A. Lupascu, S. Saito, T. Picot, P. C. de Groot, C. J. P. M. Harmans, and J. E. Mooij, Nat. Phys. **3**, 119 (2007).
[46] S. N. Shevchenko, A. S. Kiyko, A. N. Omelyanchouk, and W. Krech, Low Temp. Phys. **31**, 569 (2005).
[47] Additional investigations showed that at some detuning from the five-photon resonance, at frequency $f=1.73$ GHz of microwave field, the phase-sensitive interference between consecutive Landau-Zenner tunneling attempts was observed in the charge-phase qubit under study, by analogy with Ref. 38.